

Interacting Virtual Topological Phases in Defect-Rich 2D Materials

F. Crasto de Lima^{1,*}, Roberto H. Miwa^{2,†}, Caio Lewenkopf^{3,‡} and Adalberto Fazzio^{1,§}

¹*Illum School of Science, Brazilian Center for Research in Energy and Materials (CNPEM),
Zip Code 13083-970, Campinas, São Paulo, Brazil.*

²*Instituto de Física, Universidade Federal de Uberlândia, C.P. 593, Uberlândia, MG 38400-902, Brazil*

³*Instituto de Física, Universidade Federal Fluminense, Niterói 24210-346, Rio de Janeiro, Brazil*
(Dated: December 12, 2024)

We investigate the robustness of *virtual* topological states – topological phases away from the Fermi energy – against the electron-electron interaction and band filling. As a case study, we employ a realistic model to investigate the properties of vacancy-driven topological phases in transition metal dichalcogenides (TMDs) and establish a connection between the degree of localization of topological wave functions, the vacancy density, and the electron-electron interaction strength with the topological phase robustness. We demonstrate that electron-electron interactions play a crucial role in degrading topological phases thereby determining the validity of single-particle approximations for topological insulator phases. Our findings can be naturally extended to virtual topological phases of a wide range of materials.

Introduction.– Topological insulators (TIs) are a new class of materials that exhibit insulating bulk behavior, but conduct electricity on their surfaces [1–3], due to the presence of topologically protected metallic surface states that are robust against disorder [4–6]. This unique property, a hallmark of TIs, combined with an unusual spin texture of their topological surface states, has attracted enormous attention in the condensed matter physics and materials science [7]. Remarkably, while theory predicts thousands of materials exhibiting topological phases [8–10], the number of experimental realizations is still surprisingly small. This puzzling discrepancy can be explained, in part, by noting that approximately 88% of the predicted topological phases correspond to *virtual* electronic gaps that are energetically far from the Fermi level [8–13], requiring an electronic doping that hinders their experimental observation. However, a more fundamental challenge lies in understanding the influence of charge carrier doping and the electron-electron interaction on the electronic structure and topological properties of these materials.

For simplicity, let us focus on 2D materials. Here, as in the 3D case, numerous works have been dedicated to the study of topological-trivial/non-trivial transitions that occur as a function of temperature [14–16], external fields [17, 18], disorder [19, 20], and alloying [21–24]. However, despite the diverse range of mechanisms investigated for inducing phase transitions, the topological phase robustness with electron doping to access virtual topological states remains relatively unexplored. In this context, electron-electron repulsion plays a crucial role, particularly depending on the localization of the topological states. The competition between topological phases and interaction induced strong electronic correlations has been studied for fixed electron number within the Kane-Mele-Hubbard model [25, 26]. Our focus, instead, lies on the topological systems predicted in Refs. [8–10] which typically do not exhibit strong electronic correlations and

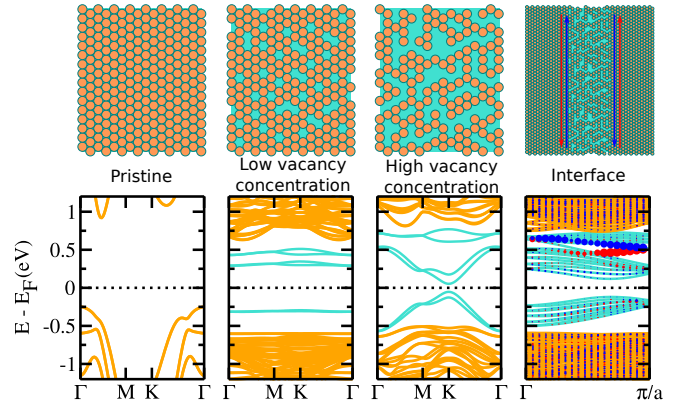


FIG. 1. Vacancy-induced topological phase in 2D MX_2 : at critical vacancy concentration, a topological gap forms, yielding spin-polarized edge states on unoccupied levels. The band structures are DFT calculations for PtSe_2 ; dashed lines mark the Fermi level; blue/red circles denote spin-up/down edge states.

can be treated within a mean-field approach.

In summary, notwithstanding the significant progress [27], the effect of electron-electron repulsion on topological gaps away from the Fermi level remains unexplored.

This Letter addresses the critical question of how electron filling influences the stability of predicted virtual topological phase transitions, revealing the conditions under which these transitions remain robust and the associated changes in the electronic band structure.

An ideal system for studying these features should allow the manipulation of wave function localization to increase electron-electron repulsion. Surprisingly, localized vacancy states in 2D-TMDs exhibit virtual non-trivial topological states that emerge beyond a critical vacancy concentration [28, 29], as shown on Fig. 1. Given the localized nature of such defect states, electron-electron repulsion can compete both with the vacancy level split-

tings [30] and the formation of a topological phase [29]. Our study explores the electron-electron repulsion in recent predicted non-trivial topological states in 2D TMDs. Through *ab initio* calculations, we demonstrate the existence of chalcogen vacancy-induced defect states in 1T-MX₂ systems, where M=Ni, Pd, Pt and X=S, Se, Te. By constructing a general minimal model within a Hubbard mean-field tight-binding approach, we validate the non-trivial/trivial phase transition in these systems as a function of the vacancy concentration and electron-electron repulsion.

Pristine MX₂ systems with light chalcogens (X=S, Se) exhibit semiconducting behavior, while MTe₂ systems (M = Ni, Pd) are metallic, with PtTe₂ remaining semiconducting [31]. To investigate the impact of chalcogen vacancies on the electronic structure, we consider a vacancy concentration n_{vac} of approximately 10^{14} cm^{-2} , a value experimentally achieved in PtSe₂ [32] and MoS₂ [33, 34]. Our calculations reveal the formation of three bands within the gap for the semiconducting systems, see Fig. 1, originating from the *d*-states of the transition metal atoms adjacent to the vacant site [35]. Given the absence of the chalcogen atom, two electrons occupy these vacancy states, resulting in a $\nu = 1/3$ filling for neutral systems.

Notably, our calculations for PtSe₂ indicate that vacancies concentrations exceeding a critical concentration of $2.5 \times 10^{14} \text{ cm}^{-2}$ [32] induce gap opening between the forth and fifth bands (at $\nu = 2/3$ filling), that are characterized as non-trivial. Since these bands are unoccupied in charge-neutral systems, this constitutes an example of a *virtual topological phase*. We employ this system as a showcase to study the influence of electron-electron repulsion on the virtual topological gap and its robustness upon filling.

Model Hamiltonian.— A minimal model to explore an insulator with virtual topological states requires at least two energy gaps, one trivial and the other non-trivial. A three orbital model is sufficient to capture the essential features of virtual topology. Specifically, for chalcogen vacancies in MX₂ systems, a three orbital model accurately describes the states close to the Fermi energy. We consider such three orbitals model, incorporating intra- and inter-vacancy orbital interactions, spin-orbit effects, and on-site Hubbard electron-electron repulsion

$$H = H_{\text{intra}} + H_{\text{inter}} + H_U. \quad (1)$$

The intra-vacancy term couples the three Pt orbitals surrounding a vacancy

$$H_{\text{intra}} = \sum_{\langle ij \rangle} \mathbf{c}_i^\dagger (t\sigma_0 + i\lambda\nu_{ij}\sigma_z) \mathbf{c}_j,$$

where t is the hopping amplitude, $\langle ij \rangle$ restricts the sum over first neighbors orbitals, λ gives the SOC strength, ν_{ij} captures the sign of the SOC term [1, 29], $\mathbf{c}_i = [c_{i\uparrow}, c_{i\downarrow}]^T$

is the annihilation operator of electron at the site/orbital i with spin projection \uparrow/\downarrow , while σ_0 and σ_z are Pauli matrices.

The inter-vacancy term couples orbitals from adjacent vacancies

$$H_{\text{inter}} = \sum_{\langle\langle ij \rangle\rangle} \mathbf{c}_i^\dagger (t'\sigma_0 + \lambda'\nu_{ij}\sigma_z) \mathbf{c}_j,$$

with the second neighbor hopping and SOC strengths given by $t' = \alpha t$ and $\lambda' = \beta \lambda$, with $0 \leq \alpha, \beta \leq 1$. α and β parameterize vacancy concentration and their spatial localization. The low n_{vac} and high n_{vac} limits correspond to $\alpha, \beta \ll 1$ and $\alpha, \beta \approx 1$, respectively. The mean-field Hubbard term reads

$$H_U = U \sum_i (n_{i\uparrow} \langle n_{i\downarrow} \rangle + n_{i\downarrow} \langle n_{i\uparrow} \rangle - \langle n_{i\uparrow} \rangle \langle n_{i\downarrow} \rangle),$$

where $n_{i\sigma} = c_{i\sigma}^\dagger c_{i\sigma}$ is the number operator and U the on-site electronic interaction energy. For finite U , the electronic problem is solved self-consistently. The matrix representation of the Hamiltonian in the three Pt-lone pair base is described in Supplemental Material [31].

Non-trivial topology.— Let us begin by discussing the simplest case where there is no inter-vacancy coupling, namely, $\alpha = \beta = 0$. In this limit the system is k -independent, and the wave functions are localized within individual vacancies. In the absence of SOC ($\lambda = 0$) and electron-electron repulsion ($U = 0$), the low energy band is doubly degenerate and the higher-energy states exhibit 4-fold degeneracy [31]. SOC lifts the 4-fold degeneracy, opening a gap that scales linearly with the SOC strength. Similarly, in the absence of SOC, the Hubbard term breaks the degeneracy between the topmost states, opening a gap that scales linearly with U . However, when both SOC and the Hubbard term are present, the gap between the top-most states scales with U as $E_{\text{gap}} \approx \sqrt{aU^2 + \lambda^2}$, where the coefficient a depends on the electron filling [31].

We analyze the system topological properties using the spin Chern number $\mathcal{C}_s = \mathcal{C}_\uparrow - \mathcal{C}_\downarrow$,

$$\mathcal{C}_\gamma = \sum_n^{\text{occup}} \oint_C \mathbf{A}_n^{(\gamma)} \cdot d\mathbf{k} \quad (2)$$

where $\gamma = \uparrow, \downarrow$ and the Berry connection $\mathbf{A}_n^{(\gamma)} = i \langle n, \mathbf{k}, \gamma | \nabla_{\mathbf{k}} | n, \mathbf{k}, \gamma \rangle$. Fully localized wave functions are eigenfunctions of the position operator $\hat{\mathbf{x}} = i \nabla_{\mathbf{k}}$, leading to a trivial topology.

Inter vacancy interactions play a crucial role in driving the topologically phase in MX₂ systems. Initially, considering $\lambda = 0.1 t$, we observe the appearance of band dispersions and associated spin Hall conductivity calculated using the Kubo formula [36, 37], as a function of α [Figs. 2 (a1)–(b3)]. For lower vacancy densities (lower α) the system exhibits a trivial virtual gap between the top-most

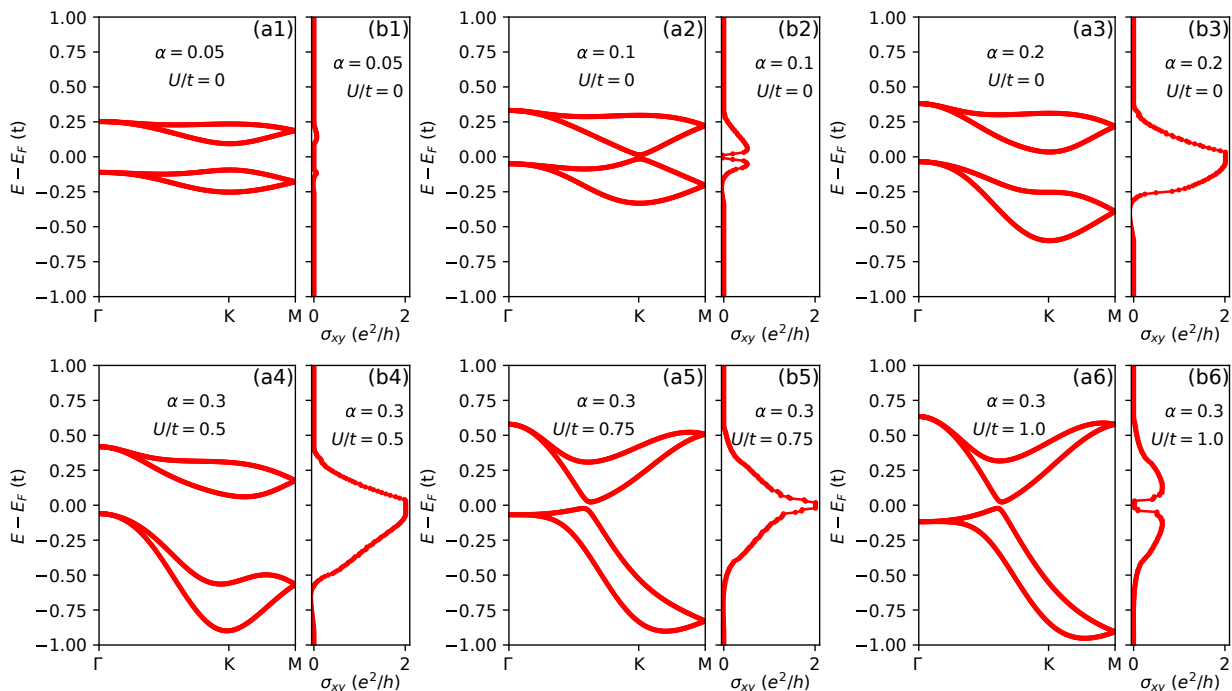


FIG. 2. Model system (a) band structure along high-symmetry direction and (b) spin Hall conductivity σ_{xy} for $\lambda = 0.1t$, and $\beta = 0$. Upper row: $U = 0$ for selected values of α . Lower row: $\alpha = 0.3$ and $\nu = 2/3$ filling for different values of U .

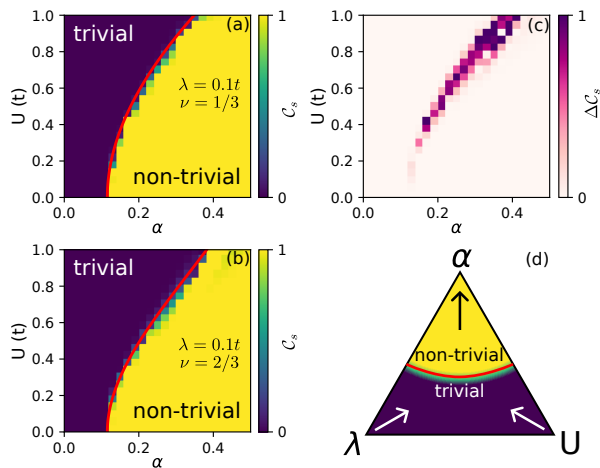


FIG. 3. Topological phase diagram of the topmost energy gap for U versus α with $\lambda = 0.1t$ for (a) $\nu = 1/3$ and (b) $\nu = 2/3$. The red lines indicate the topological transition regions where $E_{\text{gap}} \rightarrow 0$. (c) shows the difference between the phase diagrams (a) and (b). (d) Schematic phase diagram for the competition between vacancy density, SOC strength, and electron-electron interaction.

bands, as depicted in Figs. 2(a1)–(b1). The upper gap transitions to a topological phase when the inter-vacancy interaction reaches a critical value $\alpha_c = (2 - \beta)\lambda/\sqrt{3}t$. For $\beta = 0$, $\alpha_c = 2\lambda/t\sqrt{3}$ defines the critical value for the virtual gap closing and reopening at $\nu = 2/3$. Specifically, for $\lambda = 0.1t$ the critical value is $\alpha = 0.11$, as evident from the gap closing in Figs. 2(a2)–(b2). For

inter-vacancy interactions $\alpha > \alpha_c$, the system enters a non-trivial phase for $\nu = 2/3$ filling, as illustrated in Figs. 2(a3)–(b3). Interestingly, as $\alpha \rightarrow 1$ the gap at $\nu = 1/3$ filling undergoes a topological phase transition. In this limit, the system’s orbitals become the kagome lattice.

Electron-electron interaction.— Let us now consider the effect of electron-electron repulsion U and electronic filling ν on the topological properties of our model system. Our calculations reveal that, in general, the topological non-trivial phase is governed by the interplay between inter-vacancy interaction α and spin-orbit coupling λ [31], with increasing U degrading the non-trivial phase. As a specific example, let us consider a non-interacting system in a topological phase for the $\nu = 2/3$ filling, with parameters $\lambda = 0.1t$ and $\alpha = 0.3$. The effect of U on this topological phase is illustrated by the bottom row of Fig. 2. For U up to $0.5t$ the system remains with a non-trivial topological phase characterized by $\sigma_{xy} = 2e^2/h$ [Figs. 2(a4)–(b4)]. A topological phase transition occurs around $U = 0.75t$, indicated by the closing of the gap [Figs. 2(a5)–(b5)]. The gap reopens for larger U , [Figs. 2(a6)–(b6)], being trivial with $\sigma_{xy} < 2e^2/h$.

Fig. 3 shows a topological phase diagram as a function of the electron-electron repulsion U and the vacancy-vacancy interaction α for the top-most energy gap. Fig. 3(a) displays the virtual topology (at $\nu = 1/3$) phase diagram, while Fig. 3(b) shows the phase diagram for the real topology (at $\nu = 2/3$). We first notice that a topological phase emerges only for $\alpha > \alpha_c$, a criti-

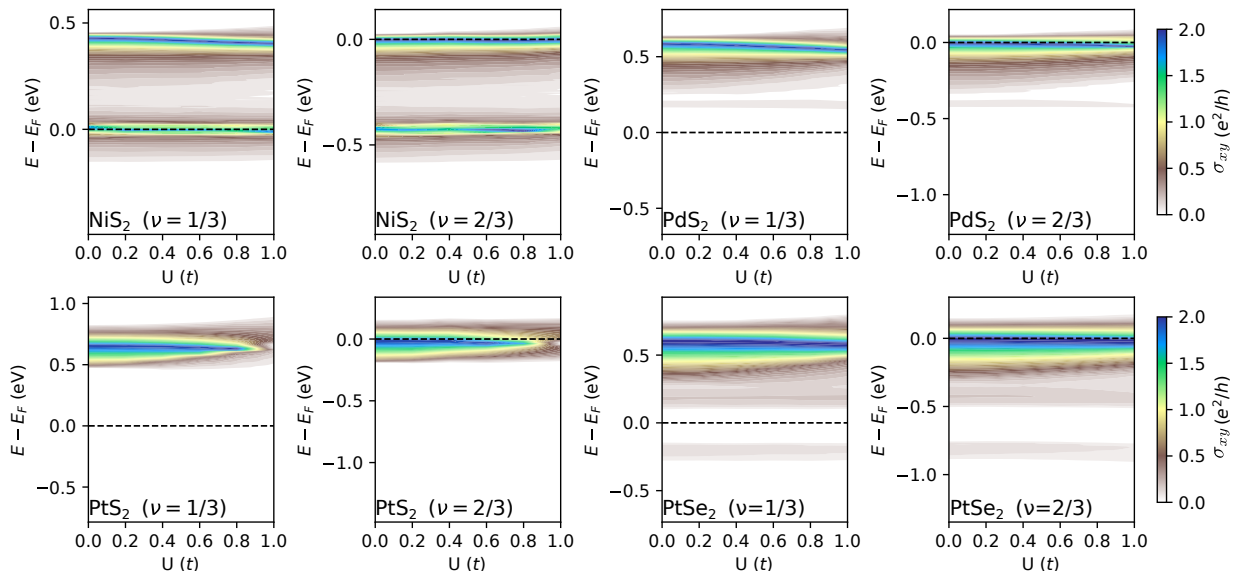


FIG. 4. Spin Hall conductivity σ_{xy} for different values of U and electron occupations ($\nu = 1/3$ and $\nu = 2/3$) in the MX_2 system. The color bars indicate the σ_{xy} values.

cal value dictated by the SOC strength λ . Increasing U drives the system towards a trivial phase. For more localized wave functions (lower α values), both in the virtual ($\nu = 1/3$) and real ($\nu = 2/3$) electron configuration exhibit similar phase diagrams. However, at higher α values, the virtual topological gap proves more robust than the real topological gap. The introduction of additional electrons enhances repulsion, further degrading the non-trivial phase. Figure 3(c) illustrates the subtraction between the real topological gap phase diagram by the virtual phase diagram, defined as $\Delta C_s \equiv C_s^{\nu=1/3} - C_s^{\nu=2/3}$. For α ranging from 0.1 to 0.4, the virtual topological phase is more robust against variation in U . In summary, the phase transition is accompanied by a gap closure governed by the competition between vacancy density, SOC, and electron-electron repulsion satisfying the approximate relation, $E_{\text{gap}} \approx [aU^2 + \lambda^2 - (\alpha t \sqrt{3}/2)^2]^{1/2}$. The gap closure, $E_{\text{gap}} = 0$, is represented by the red curves in Figs. 3(a) and (b), corresponding to the topological phase transition condition. Here, as before, a is a parameter that depends on ν . Figure 3(d) presents a ternary diagram visualizing the topological phase behavior. Increasing the vacancy density stabilizes the non-trivial phase, while stronger SOC and electron-electron repulsion tend to drive the system towards a trivial phase.

Topological robustness.— Now, we focus on realistic TMD calculations with vacancy states in the semiconducting gap, enabling a topological insulating phase. We identify such systems using density functional theory (DFT) calculations [31], with the extracted the corresponding tight-binding parameters for H_{intra} and H_{inter} [Table I]. To address the uncertainties in the Hubbard U -value, particularly with electron doping, we extract

our model parameters using $U = 0$ DFT, effectively capturing the screened electronic interactions in the weak electronic correlations regime [38, 39], and systematically vary U . Given the nature of SOC, its strength is larger for heavier transition metals, ranging from 7% to 18% of the hopping strength. The vacancy concentration dictates the proximity of adjacent vacancies and, consequently, the (second-neighbor) inter-vacancy decaying factors, α and β . The later are obtained from DFT calculations for $n_{\text{vac}} = 10^{14} \text{ cm}^{-2}$ [23, 32]. For such concentration, α ranges from 0.37 for PtS_2 to nearly 1.00 for NiS_2 . This variation in α reflects the localization of the defect wave function, being less localized in the NiS_2 system. Due to the dielectric nature of the MX_2 , the screening of the SOC field leads to $\beta \rightarrow 0$, validating our previous discussion.

TABLE I. Model parameters extracted from DFT calculations [31] for $n_{\text{vac}} = 10^{14} \text{ cm}^{-2}$.

MX_2	t (eV)	α	λ (eV)	β
NiS_2	0.15	0.99	0.01	0.03
PdS_2	0.26	0.58	0.02	-0.05
PtS_2	0.36	0.37	0.06	-0.10
PtSe_2	0.28	0.61	0.05	0.08

Figure 4 shows the calculated spin Hall conductivity for the TMD systems [parameter in Table I] for different values of U and both $\nu = 1/3$ and $\nu = 2/3$ fillings. The robustness of the topological phase with respect to U is directly correlated with the vacancy state localization. Less localized systems, such as NiS_2 , exhibit a topological phase robust up to $U = t$, while in the more localized systems, PtS_2 , the topological phase vanishes for $U > 0.6t$.

Comparing the robustness of the topological states at $\nu = 1/3$ filling with $\nu = 2/3$ fillings, we find that the more localized systems exhibit a virtual topological phase more robust than the real topological state. For instance, in PtS₂, the non-trivial phase degrades with lower U . These findings support our discussion of the topological phase diagrams shown in Fig. 3.

Conclusions.— Our study reveals that electron-electron interactions significantly impact the stability of topological phases, particularly the transition between virtual and real of topological states upon electron filling. As a case study, we demonstrated that in 2D TMDs with vacancy-induced topological phases, the robustness of these virtual/real phases is influenced by a complex interplay between vacancy density, spin-orbit coupling, and electron-electron repulsion. While higher vacancy concentrations can enhance the non-trivial topology, electron-electron interactions may suppress the topological phase, drastically reducing the number of possible experimental realizations of TIs. These findings provide a comprehensive understanding on the interaction between electron filling, vacancy concentration, and topological protection in TMDs, highlighting the possibility of tuning topological phases in other materials through vacancy engineering and controlled doping.

Acknowledgments.— The authors acknowledge financial support from the Brazilian agencies FAPESP, CNPq (INCT - Materials Informatics), FAPERJ, and LNCC (Laboratório Nacional de Computação Científica) for computer time (Project ScafMat2).

* felipe.lima@ilum.cnpem.br

† hiroki@ufu.br

‡ caio.lewenkopf@id.uff.br

§ adalberto.fazzio@ilum.cnpem.br

- [1] C. L. Kane and E. J. Mele, Quantum Spin Hall Effect in Graphene, *Phys. Rev. Lett.* **95**, 226801 (2005).
- [2] B. A. Bernevig, T. L. Hughes, and S.-C. Zhang, Quantum Spin Hall Effect and Topological Phase Transition in HgTe Quantum Wells, *Science* **314**, 1757 (2006).
- [3] L. Fu, C. L. Kane, and E. J. Mele, Topological Insulators in Three Dimensions, *Phys. Rev. Lett.* **98**, 106803 (2007).
- [4] M. Z. Hasan and C. L. Kane, Colloquium: Topological insulators, *Rev. Mod. Phys.* **82**, 3045 (2010).
- [5] X.-L. Qi and S.-C. Zhang, Topological insulators and superconductors, *Rev. Mod. Phys.* **83**, 1057 (2011).
- [6] R. Moessner and J. E. Moore, *Topological Phases of Matter* (Cambridge University Press, 2021).
- [7] O. Breunig and Y. Ando, Opportunities in topological insulator devices, *Nat. Rev. Phys.* **4**, 184 (2022).
- [8] T. Zhang, Y. Jiang, Z. Song, H. Huang, Y. He, Z. Fang, H. Weng, and C. Fang, Catalogue of topological electronic materials, *Nature* **566**, 475 (2019).
- [9] M. Vergniory, L. Elcoro, C. Felser, N. Regnault, B. Andrei Bernevig, and Z. Wang, A complete catalogue of high-quality topological materials, *Nature* **566**, 480 (2019).
- [10] F. Tang, H. Po, A. Vishwanath, and X. Wan, Comprehensive search for topological materials using symmetry indicators, *Nature* **566**, 486 (2019).
- [11] M. G. Vergniory, B. J. Wieder, L. Elcoro, S. S. P. Parkin, C. Felser, B. A. Bernevig, and N. Regnault, All topological bands of all nonmagnetic stoichiometric materials, *Science* **376**, eabg9094 (2022).
- [12] J. Kruthoff, J. de Boer, J. van Wezel, C. L. Kane, and R.-J. Slager, Topological Classification of Crystalline Insulators through Band Structure Combinatorics, *Phys. Rev. X* **7**, 041069 (2017).
- [13] R.-J. Slager, A. Mesaros, V. Juričić, and J. Zaanen, The space group classification of topological band-insulators, *Nat. Phys.* **9**, 98 (2012).
- [14] B. Monserrat and D. Vanderbilt, Temperature Effects in the Band Structure of Topological Insulators, *Phys. Rev. Lett.* **117**, 226801 (2016).
- [15] B. Focassio, G. R. Schleder, F. Crasto de Lima, C. Lewenkopf, and A. Fazzio, Amorphous Bi₂Se₃ structural, electronic, and topological nature from first principles, *Phys. Rev. B* **104**, 214206 (2021).
- [16] S. Chen, I. J. Parker, and B. Monserrat, Temperature effects in topological insulators of transition metal dichalcogenide monolayers, *Phys. Rev. B* **109**, 155125 (2024).
- [17] M. Kim, C. H. Kim, H.-S. Kim, and J. Ihm, Topological quantum phase transitions driven by external electric fields in Sb₂Te₃ thin films, *Proc. Natl. Acad. Sci. U.S.A.* **109**, 671 (2011).
- [18] Q. Liu, X. Zhang, L. B. Abdalla, A. Fazzio, and A. Zunger, Switching a Normal Insulator into a Topological Insulator via Electric Field with Application to Phosphorene, *Nano Lett.* **15**, 1222 (2015).
- [19] B. D. Assunção, G. J. Ferreira, and C. H. Lewenkopf, Phase transitions and scale invariance in topological anderson insulators, *Phys. Rev. B* **109**, L201102 (2024).
- [20] V. Regis, V. Velasco, M. B. S. Neto, and C. Lewenkopf, Structure-driven phase transitions in paracrystalline topological insulators, *Phys. Rev. B* **110**, L161105 (2024).
- [21] F.-C. Chuang, C.-H. Hsu, H.-L. Chou, C. P. Crisostomo, Z.-Q. Huang, S.-Y. Wu, C.-C. Kuo, W.-C. V. Yeh, H. Lin, and A. Bansil, Prediction of two-dimensional topological insulator by forming a surface alloy on Au/Si(111) substrate, *Phys. Rev. B* **93**, 035429 (2016).
- [22] C.-L. Zhang, T. Liang, N. Ogawa, Y. Kaneko, M. Kriener, T. Nakajima, Y. Taguchi, and Y. Tokura, Highly tunable topological system based on PbTe-SnTe binary alloy, *Phys. Rev. Mater.* **4**, 091201 (2020).
- [23] F. Crasto de Lima, B. Focassio, R. H. Miwa, and A. Fazzio, Topological insulating phase arising in transition metal dichalcogenide alloy, *2D Mater.* **10**, 035001 (2023).
- [24] T. Mota, L. K. Teles, F. Matusalem, and I. Guilhon, Thermodynamic and electronic properties of (Bi_{1-x}Sb_x)₂Se₃ topological insulator alloy, *Phys. Rev. B* **109**, 235150 (2024).
- [25] S. Rachel and K. Le Hur, Topological insulators and Mott physics from the Hubbard interaction, *Phys. Rev. B* **82**, 075106 (2010).
- [26] M. Hohenadler, T. C. Lang, and F. F. Assaad, Correlation Effects in Quantum Spin-Hall Insulators: A Quantum Monte Carlo Study, *Phys. Rev. Lett.* **106**, 100403 (2011).

- (2011).
- [27] S. Rachel, Interacting topological insulators: a review, *Reports on Progress in Physics* **81**, 116501 (2018).
- [28] F. C. de Lima, G. J. Ferreira, and R. H. Miwa, Tuning the topological states in metal-organic bilayers, *Phys. Rev. B* **96**, 115426 (2017).
- [29] F. Crasto de Lima and A. Fazzio, At the Verge of Topology: Vacancy-Driven Quantum Spin Hall in Trivial Insulators, *Nano Lett.* **21**, 9398 (2021).
- [30] M. A. U. Absor, I. Santoso, Harsojo, K. Abraha, F. Ishii, and M. Saito, Defect-induced large spin-orbit splitting in monolayer PtSe₂, *Phys. Rev. B* **96**, 115128 (2017).
- [31] See Supplemental Material at [URL will be inserted by publisher] for a description of the *ab initio* calculations, the extraction of model Hamiltonian parameters, and a detailed analysis of the single-vacancy model.
- [32] X. Lin, J. C. Lu, Y. Shao, Y. Y. Zhang, X. Wu, J. B. Pan, L. Gao, S. Y. Zhu, K. Qian, Y. F. Zhang, D. L. Bao, L. F. Li, Y. Q. Wang, Z. L. Liu, J. T. Sun, T. Lei, C. Liu, J. O. Wang, K. Ibrahim, D. N. Leonard, W. Zhou, H. M. Guo, Y. L. Wang, S. X. Du, S. T. Pantelides, and H.-J. Gao, Intrinsically patterned two-dimensional materials for selective adsorption of molecules and nanoclusters, *Nat. Mater.* **16**, 717 (2017).
- [33] H. Li, C. Tsai, A. L. Koh, L. Cai, A. W. Contryman, A. H. Fragapane, J. Zhao, H. S. Han, H. C. Manoharan, F. Abild-Pedersen, J. K. Nørskov, and X. Zheng, Activating and optimizing MoS₂ basal planes for hydrogen evolution through the formation of strained sulphur vacancies, *Nat. Mater.* **15**, 48 (2015).
- [34] H.-P. Komsa, J. Kotakoski, S. Kurasch, O. Lehtinen, U. Kaiser, and A. V. Krasheninnikov, Two-Dimensional Transition Metal Dichalcogenides under Electron Irradiation: Defect Production and Doping, *Phys. Rev. Lett.* **109**, 035503 (2012).
- [35] R. L. H. Freire, F. C. de Lima, and A. Fazzio, Vacancy localization effects on MX₂ transition-metal dichalcogenides: A systematic *ab initio* study, *Phys. Rev. Mater.* **6**, 084002 (2022).
- [36] J. Sinova, D. Culcer, Q. Niu, N. A. Sinitsyn, T. Jungwirth, and A. H. MacDonald, Universal Intrinsic Spin Hall Effect, *Phys. Rev. Lett.* **92**, 126603 (2004).
- [37] L. Matthes, S. Küfner, J. Furthmüller, and F. Bechstedt, Intrinsic spin Hall conductivity in one-, two-, and three-dimensional trivial and topological systems, *Phys. Rev. B* **94**, 085410 (2016).
- [38] M. S. Hybertsen, M. Schlüter, and N. E. Christensen, Calculation of Coulomb-interaction parameters for La₂CuO₄ using a constrained-density-functional approach, *Phys. Rev. B* **39**, 9028 (1989).
- [39] G. A. Baraff, E. O. Kane, and M. Schlüter, Silicon Vacancy: A Possible "Anderson Negative-*U*" System, *Phys. Rev. Lett.* **43**, 956 (1979).